

ACCEPTED MANUSCRIPT

# Growth of L-asparagine monohydrate and its structural, optical, mechanical, thermal and electrical studies for nonlinear optical applications

To cite this article before publication: Apurva Gupta *et al* 2020 *Mater. Res. Express* in press <https://doi.org/10.1088/2053-1591/ab7a5d>

## Manuscript version: Accepted Manuscript

Accepted Manuscript is “the version of the article accepted for publication including all changes made as a result of the peer review process, and which may also include the addition to the article by IOP Publishing of a header, an article ID, a cover sheet and/or an ‘Accepted Manuscript’ watermark, but excluding any other editing, typesetting or other changes made by IOP Publishing and/or its licensors”

This Accepted Manuscript is © 2020 IOP Publishing Ltd.

During the embargo period (the 12 month period from the publication of the Version of Record of this article), the Accepted Manuscript is fully protected by copyright and cannot be reused or reposted elsewhere.

As the Version of Record of this article is going to be / has been published on a subscription basis, this Accepted Manuscript is available for reuse under a CC BY-NC-ND 3.0 licence after the 12 month embargo period.

After the embargo period, everyone is permitted to use copy and redistribute this article for non-commercial purposes only, provided that they adhere to all the terms of the licence <https://creativecommons.org/licenses/by-nc-nd/3.0>

Although reasonable endeavours have been taken to obtain all necessary permissions from third parties to include their copyrighted content within this article, their full citation and copyright line may not be present in this Accepted Manuscript version. Before using any content from this article, please refer to the Version of Record on IOPscience once published for full citation and copyright details, as permissions will likely be required. All third party content is fully copyright protected, unless specifically stated otherwise in the figure caption in the Version of Record.

View the [article online](#) for updates and enhancements.

# Growth of L-asparagine Monohydrate and its Structural, Optical, Mechanical, Thermal and Electrical Studies for Nonlinear Optical Applications

Apurva Gupta<sup>1</sup>, Raseel Rahman M.K.<sup>1</sup>, RO. MU. Jauhar<sup>2</sup>, V. Sivasubramani<sup>3</sup>, N. Vijayan<sup>4</sup>, G. Vinitha<sup>2</sup>, Lekha Nair<sup>1\*</sup>

<sup>1</sup> Department of Physics, Jamia Millia Islamia, New Delhi-110025, India

<sup>2</sup> Division of Physics, School of Advanced Sciences, Vellore Institute of Technology, Chennai – 600127, India

<sup>3</sup> Research Centre, SSN College of Engineering, Kalavakkam, Chennai 603110, India

<sup>4</sup> CSIR- National Physical Laboratory, Dr. K. S. Krishnan Road, New Delhi-110012, India

Email id: [lnair@jmi.ac](mailto:lnair@jmi.ac)

ORCID ID: 0000-0003-4266-9143

## Abstract

In the recent past, single crystals of organic materials exhibiting nonlinear optical behaviour have garnered much attention in the field of optical data storage and laser technology. In the present article, amino acid crystals of L-asparagine monohydrate (LAM) have been grown successfully by conventional slow evaporation solution growth technique from aqueous solution at room temperature (RT), with double distilled water used as a solvent. Single crystal X-ray diffraction was used to confirm the orthorhombic crystal structure (with  $P2_12_12_1$  space group) and lattice parameters of the grown crystal were determined. The crystallinity, purity, and phase of L-asparagine monohydrate were also determined from the powder X-ray diffraction data. The optical behaviour of LAM crystals was investigated by UV-Visible-NIR spectroscopy, and no absorption was found in the entire visible region. From the Tauc plot, the optical energy band gap was evaluated to be 5.09 eV. Valence band ( $E_{VB}$ ) and conduction band ( $E_{CB}$ ) positions of LAM were calculated from the knowledge of electron affinity ( $E_a$ ), ionisation energy ( $E_i$ ) of the elements and optical energy gap. Thermal parameters of the crystal were measured by photoacoustic spectroscopy. In addition, the mechanical stability of L-asparagine monohydrate single crystal was evaluated via shock damage threshold measurement. The dielectric studies as a function of frequency and temperature were carried out to understand the electrical behavior of the grown crystal. From the Z-scan analysis, nonlinear refractive index ( $n_2$ ) and nonlinear absorption coefficient ( $\beta$ ) of the LAM crystal were also determined.

**Keywords:** NLO single crystal; L-asparagine; XRD; Shock damage threshold; Photoacoustic measurement.

## 1. Introduction

In the past few decades, the development of standardized methods of single crystal growth has tremendous impact in various fields like photonics, optoelectronics, semiconductor technology etc. [1, 2]. Inorganic single crystals such as KDP (abbreviation of potassium dihydrogen orthophosphate,  $KH_2PO_4$ ) and  $LiNbO_3$  (lithium niobate) have been the foundation

on which optical communications have been developed, but recently, organic crystals with highly anisotropic optical response have become increasingly important [3]. The degree of charge separation (polarization) which is induced by energy and intensity of the incident light is responsible for the optical properties of these NLO materials. The NLO activity is enhanced in organic material as compared to inorganic material due to the presence of the conjugated  $\pi$ -electron system, containing donor and acceptor groups [4]. NLO activity in inorganic materials such as  $\text{LiNbO}_3$ ,  $\text{LiTaO}_3$  and KDP originates from their ionic bonding. In organic materials, the molecules are connected with weak van der Waals and hydrogen bonds, resulting in greater structural diversity and ease of design and fabrication [5-7]. Among these, the amino acids crystals exhibit fascinating NLO properties. Usually, amino acid-based compounds crystallize in a non-centrosymmetric (NCS) crystal system, which is a key requirement for demonstrating second harmonic generation (SHG).

L-asparagine, with 20 amino acids, is one such promising organic NLO material, with space group  $P2_12_12_1$  [8, 9] and possessing 4 molecules in the unit cell. Some other names of this compound are 2-Amino-3-carbamoyl propanoic acid, (S)-(+)-2-Amino succinamic acid, monohydrated (S) - 2-Aminosuccinic acid 4-amide, and L-Aspartic acid 4-amide. Its second harmonic generation (SHG) response has been found to be 0.32 times that of KDP [10]. Amino acids contain two groups: carboxyl group ( $-\text{COOH}$ ) and amino group ( $-\text{NH}_2$ ) and in the solid state, the carboxylic group behaves as a proton donor and amino group acts as a proton acceptor, and forms ( $\text{COO}^-$ ) and ( $\text{NH}_3^+$ ), within the molecule to establish the dipole nature of the compound [11-13]. Because of this dipole nature of amino acids, we come across some fascinating physical and chemical properties with their NLO behaviour making them appropriate candidates for applications. Hence, it is the need of the hour to produce good quality defect free single crystals to fulfill this aim. There are few reports of detailed determination of the optical behaviour, shock damage threshold (SDT), photoacoustic measurements (PAM) etc. for LAM, which are essential parameters for fabricating devices.

In the present study, we achieve the growth of L-asparagine monohydrate (LAM) single crystal by using a conventional slow evaporation solution growth technique (SEST) from aqueous solution at room temperature (RT). The LAM crystals are analysed by using single crystal X-ray diffraction (SCXRD), powder X-ray diffraction (PXRD), UV-Visible-NIR spectroscopy, shock damage threshold, photoacoustic measurement, photoconductivity, dielectric studies (DS) and Z-scan studies.

## 2. Experimental

### 2.1 Crystal growth

Commercially available L-asparagine monohydrate salt (LOBA Chemie, 99 %) is dissolved in double distilled water. For making a homogeneous solution, the solution was continuously stirred for the period of 26 hours at  $40^\circ\text{C}$  by using a magnetic stirrer. Then the prepared homogeneous solution of L-asparagine monohydrate was filtered by using Grade 1 Whatman filter paper (pore size  $11\mu\text{m}$  and thickness  $180\mu\text{m}$ ), to extract the impurities from the solution. A beaker

1  
2 containing filtered homogeneous solution was covered with a perforated thin plastic sheet for avoiding dust particles,  
3  
4 with a few pinholes made for evaporation, and kept at RT. After a period of 45 days, single crystals of LAM were obtained  
5  
6 from the solution. To get a flat surface, grown crystals of LAM were well polished with double distilled water (Fig. 1)  
7  
8 and then subjected to characterisations to examine its structural, optical, mechanical, thermal, electrical, and nonlinear  
9  
10 optical properties.

## 11 12 13 **2.2 Characterization Techniques**

14  
15 Single crystal X-ray diffraction (SCXRD) of the grown crystal was performed using a Bruker AXS Kappa single  
16  
17 crystal (D8 QUEST) diffractometer equipped with CMOS detector, with graphite monochromatic MoK $\alpha$  radiation source  
18  
19 ( $\lambda = 0.71073 \text{ \AA}$ ) at RT. Powder XRD was analysed using the Rigaku smart lab X-ray diffractometer with CuK $\alpha$  radiation  
20  
21 ( $\lambda=1.54059 \text{ \AA}$ ) at RT, with an electron current of 30 mA and voltage 40 kV. The sample was scanned in the continuous  
22  
23 scan mode with  $2\theta$  ranging from 5-90° at a scan speed of 3°/minute, with 0.02° step size. For the optical study, UV-Visible-  
24  
25 NIR spectral analysis was performed using the spectrophotometer of Perkin Elmer Lambda 35 over the wavelength range  
26  
27 from 200 nm to 1100 nm at room temperature. A semiautomatic shock tube which can generate shock waves from 1.2 to  
28  
29 4.5 Mach number was used for mechanical characteristics. An in-house-developed photoacoustic spectrophotometer was  
30  
31 used for measuring the thermal parameters of the grown LAM crystals. A 250 W halogen lamp was employed as a light  
32  
33 source. At RT, both photo current and dark current were measured using the Keithley pico-ammeter (MODEL M 6487)  
34  
35 for applied voltages of 0-50 volts (V) in step of 1 volt. For electrical study, PSM 1735 LCR instrument was used for  
36  
37 dielectric measurement at different temperature range as a function of frequency range from 2 kHz to 1 MHz. A continuous  
38  
39 wave (CW) neodymium-doped yttrium aluminium garnet (Nd: YAG) laser radiation of wavelength 532 nm with input  
40  
41 power 100 mW was used to execute the Z-scan experiment for the grown LAM crystal in the present study. The laser  
42  
43 beam was focused using a 10.1 cm focal length (L) lens.

## 44 45 46 47 48 **3. Results and discussion**

### 49 50 **3.1. Single crystal X-ray diffraction (SCXRD) analysis**

51  
52 The lattice parameters are obtained using the Apex III suites software as  $a = 5.5963 \text{ \AA}$ ,  $b = 9.8407 \text{ \AA}$ ,  $c = 11.8076 \text{ \AA}$ ,  
53  
54  $\alpha = 90^\circ$ ,  $\beta = 90^\circ$ ,  $\gamma = 90^\circ$  and  $V = 650.26 \text{ \AA}^3$  with the orthorhombic crystal structure system and P2<sub>1</sub>2<sub>1</sub>2<sub>1</sub> space group, which  
55  
56 is in concurrence with the reported values [14], as given in Table 1.  
57  
58  
59  
60

### 3.2. Powder X-ray diffraction (PXRD) study

PXRD analysis is the most powerful method for determining the crystallinity, phase and purity of the grown compound. For measurement, initially, a grown crystal is crushed with the help of agate mortar and pestle, and made into a fine powder. The obtained diffraction pattern is presented in Fig. 2. In Fig. 2, we observe that the peaks are sharp with no broadening, indicating the high crystallinity that is obtained. As per the crystallographic notation, the diffraction peaks corresponding to (h k l) plane such as (011), (110), (121), (113), (201), (104), (212), (220), (231), (201), (104), (212), (220), (124), (222), (231), (134), (321), and (321) are indexed and the maximum intensity peaks are found correspond to (113) plane, which is labeled as the 100% peak.

### 3.3. UV-Visible-NIR spectroscopy studies

UV-Visible-NIR spectrophotometry is an efficient technique used to investigate the optical properties of materials such as optical transition type, electronic band structure, absorption coefficient etc. [15, 16]. For UV-Visible measurement, well-polished 2 mm thick optically transparent LAM wafer is used to record the transmittance spectrum. The obtained transmittance spectrum of LAM single crystal is displayed in Fig. 3 (a) which indicates that the LAM crystals have a 'lower cut-off wavelength' at 240 nm and the crystal indicates ~ 80 % transmittance without any significant absorption in the entire UV-Visible-NIR range [250-1100 nm]. Thus, the crystal has good optical behaviour along with lower cutoff wavelength which is a measure of the potential of this material to be used in optoelectronic and NLO applications [17, 18].

#### 3.3.1 Optical absorption coefficient

For materials, the absorption coefficient ( $\alpha$ ) varies with the incident photon energies and for different wavelength  $\alpha$  it can be estimated by the transmittance data using the following relation [19, 20]:

$$\alpha = \frac{2.303 \cdot \log\left(\frac{1}{T}\right)}{t} \quad (1)$$

where  $t$  the sample thickness (2 mm) and  $T$  is the transmittance. The optical energy bandgap of grown LAM single crystal is calculated using the Tauc's plot ( $(\alpha h\nu)^2$  on the y-axis versus photon energy ( $h\nu$ ) on the x-axis), as illustrated in Fig. 3 (b). The dependence of the optical absorption strength depends on the difference between the photon energy and band gap as [21-26]:

$$\alpha h\nu = A(h\nu - E_g)^n \quad (2)$$

where  $h$  is Planck's constant ( $6.626 \times 10^{-34}$  joule-seconds),  $\nu$  is the incident photon frequency,  $A$  is constant,  $E_g$  is the optical energy bandgap, and  $n$  is an index. The value of  $n$  signifies the type of allowed electronic transitions, with value

1  
2  $n = 1/2$  for direct allowed transition,  $n = 2$  for an indirect allowed transition,  $n = 3$  for forbidden indirect transition, and  $n$   
3  
4  $= 3/2$  for forbidden direct transition [23]. The tangent line from the linear region in the graph is used to determine the  
5  
6 band gap value as its intercept at the X-axis. For the LAM crystal of this study,  $(\alpha h\nu)^2$  is used (with  $n = 1/2$ ) which shows  
7  
8 the direct allowed transition [24]. From the Tauc plot, the value of optical energy bandgap ( $E_g$ ) for LAM crystal is obtained  
9  
10 to be 5.09 eV in Fig. 3 (b), which is comparable with values from the literature of 5.1 eV and 5.08 eV references [24].  
11  
12 Theoretically, the optical band gap energy value can be calculated by using the equation:

$$E_g = hc/\lambda_{max} \quad (3)$$

13  
14 where  $c$  is the light speed in vacuum and  $\lambda_{max}$  is cutoff wavelength (240 nm for LAM crystal). From the equation (3),  
15  
16 the obtained energy band gap value is measured 5.17 eV which is close to our experimental value.  
17  
18  
19  
20

### 21 3.3.2 Determination of valence band position and conduction band position

22  
23 For compound materials in the solid state, the conduction band ( $E_{CB}$ ) and valence band ( $E_{VB}$ ) positions can be  
24  
25 estimated by using the values of ionization energy ( $E_i$ ) and electron affinity ( $E_a$ ), if the order of its elements are known.  
26  
27 In the present work, the LAM crystal is made up of such elements like carbon (C), hydrogen (H), nitrogen (N), and oxygen  
28  
29 (O), with the orders as 4 for carbon, 10 for hydrogen, 2 for nitrogen, and 4 for oxygen. The indices  $i$ ,  $j$ ,  $k$ , and  $l$  denote the  
30  
31 orders of C, H, N, and O atoms, respectively. The position of conduction band potential ( $E_{CB}$ ) is calculated by using the  
32  
33 empirical relation such as [27-30]:

$$E_{CB} = E^e - X + \frac{E_g}{2} \quad (4)$$

$$\text{where } X = [(X_C)^i \times (X_H)^j \times (X_N)^k \times (X_O)^l]^{1/(i+j+k+l)} \quad (5)$$

$$X_M = \frac{(E_{aM} + E_{iM})}{2} \quad (6)$$

34  
35  
36 where,  $M = C, H, N,$  and  $O,$  respectively and  $E_{CB}$  is the energy of conduction band potential,  $E_g$  is the optical  
37  
38 energy bandgap of LAM crystal (5.09 eV),  $E^e$  is the dissociation energy of the hydrogen molecules which is equal to  
39  
40 4.47 eV [31], and  $X$  is the energy parameter. By putting these constant values of electron affinity ( $E_a$ ) and ground state  
41  
42 ionization energy ( $E_i$ ) in terms of eV of C, H, N, and O, the energy parameter ( $X$ ) can be calculated from the equation 5.  
43  
44 The value of electron affinity ( $E_a$ , eV) are 1.595 (C), 0.754 (H), 0.073 (N) and 1.461 (O), and the value of ground state  
45  
46 ionization energy ( $E_i$ , eV) are 11.26 (C), 13.598 (H), 14.533 (N), and 13.617 (O), respectively. The conduction band ( $E_{CB}$ )  
47  
48 and valence band energy ( $E_{VB}$ ) positions are observed to be - 0.087 eV and 5.003 eV, respectively, which are displayed in  
49  
50  
51  
52  
53  
54  
55 Fig. 4.  
56  
57  
58  
59  
60

### 3.4. Shock damage threshold measurement

To determine the mechanical characteristics of the crystals for their performance in device applications, shock damage threshold measurement (SDT) is carried out, which is a unique technique to understand the behavior of the crystals at extreme conditions. Formation of shock waves leads to energy release in the form of sharp increase in temperature and pressure, like an explosion [32-33]. Generally, the nature of the shock wave is destructive [34]. A transparent and good quality LAM crystal (with size  $5 \times 5 \times 2 \text{ mm}^3$ ) is located in the sample holder that is fixed at 1 cm away from the open end of the driven section and the shock pulses are loaded on the crystal by varying the Mach number from 1.2 to 2.2. After each shock, the crystal surface is carefully checked using an optical microscope (WESWOX, BXLTR, 2010) to confirm the damage. Figure 5 (a) illustrates the surface of the crystal before loading the shock waves. Interestingly, no visible damage is observed after loading of shock pulses with Mach numbers 1.2, 1.5, 1.8 and 2.0. When the Mach number (Ma) is increased to 2.2 which corresponds to a transient pressure of 2.040 MPa and transient temperature of 864 K, clear changes are detected on the surface of the LAM crystal as illustrated in Fig. 5 (b). It is clear that a number of bubble-like projections appeared on the surface of the crystal. Then, the Mach number 2.2 is fixed and continuous pulses are loaded on the sample. When the number of shock pulses increased one by one, the concentration of the defect points also increased (Fig. 5 (c-g)). After the 15<sup>th</sup> shock, the crystal has cracked, as illustrated in Fig. 5 (h & i). Since this crystal could withstand up to 2.0 Mach number, it is determined that this crystal can be used in vibrating and fast-moving devices.

### 3.5. Photoacoustic measurement

Photoacoustic spectroscopy (PAS) is a nondestructive tool to measure thermophysical properties of material like solid, liquid and gases. During this, the light energy absorbed from the sample is converted to heat energy, causing pressure fluctuation in the surrounding air [35-36]. At modulation frequency, a microphone takes the pressure fluctuation as an acoustic signal. The crystal is positioned in a photoacoustic (PA) cell and a sensitive microphone is used as a detector. A chopper is fixed in front of the sample for capturing the modulated signal. The spectrophotometer is calibrated with the standard material like KDP, quartz and BK7 glass with a dimension of up to ( $10 \times 10 \times 1 \text{ mm}^3$ ). A light beam produced from the lamp is collimated and modulated, and it enters into the sample, generating a PA signal, and these signals are detected by the microphone. With the help of a computer using sound recording software, the resultant PA signal is documented. In our study, a crystal of LAM with dimensions of  $4 \times 4.1 \times 1.3 \text{ mm}^3$  is placed for measurement. The PA signal recorded with different-2 chopping frequency from 10 to 120 Hertz (Hz). The graph of normalized amplitude of photoacoustic (PA) signal versus square root of chopping frequency ( $f^{1/2}$ ) is plotted and is displayed in Fig. 6. In this

graph, we observed that as chopping frequency is increased, the normalized amplitude of photoacoustic (PA) signal is decreased considerably.

The thermal diffusivity ( $\alpha$ ) of the sample is estimated from the curve fitting method [37- 41]. The thermal effusivity ( $e$ ) and conductivity ( $k$ ) of the specimen are calculated with the help of thermal diffusivity value ( $\alpha$ ) using the following relations as:

$$k = \alpha\rho C_p \quad (7)$$

and

$$e = \rho C_p \alpha^{1/2} \quad (8)$$

where  $k$  denotes thermal conductivity,  $\alpha$  denotes thermal diffusivity,  $\rho$  denotes the density,  $e$  is the thermal effusivity and  $C_p$  is the specific heat capacity of the crystal, respectively. The measured thermal parameters i.e.  $k$ ,  $\alpha$ , and  $e$  are cited in Table 2. The higher values of thermal parameters of the crystal indicate that the crystal may be used for high power laser action [35].

### 3.6. Photoconductivity measurement

For measurement, a good quality polished LAM crystal is chosen and two electrodes are made on the surface of crystal at a finite distance (1 mm) by using the high grade silver paste. After that, the crystal is fixed inside a cryostat which is evacuated to  $10^{-6}$  mbar vacuum. For the measurement of photocurrent ( $I_p$ ), the sample is exposed to 50 W halogen lamp which acts as a source of radiation and dark current ( $I_d$ ) is reported when the lamp is in the off condition. From Fig. 7, we observed that the photocurrent ( $I_p$ ) is less than the dark current ( $I_d$ ) for different applied fields. This indicates that the LAM single crystal shows the negative photoconductivity. Usually, the loss of water molecules in the crystal may be responsible for showing the negative photoconductivity [42]. However, under illumination the decrease in the number of charge carriers (CCs) or their lifetime give rise to negative photoconductivity. According to this relation the lifetime,  $\tau = (v\sigma N)^{-1}$  (where  $v$  denotes the thermal speed of charge carriers,  $\sigma$  denotes the capture cross-section of the recombination centers, and  $N$  denotes the carrier concentration). Under illumination, the decrease in the lifetime occurs with an increase in applied voltage, due to a rise in carrier velocity and possibility increases the trapping [43].

By the Stockman model, the phenomena of negative photoconductivity could be explained in detail with the two level scheme [44]. According to this scheme, there exist two energy states within the forbidden bandgap, one lies between the Fermi level and conduction band edge ( $E_{CB}$ ), which is denoted as the upper energy level, while the other is in proximity to the valence band edge ( $E_{VB}$ ) or in between Fermi level and valence band edge, and is called lower energy level. The second level has a higher capture cross section for charge carriers (i.e. holes and electrons). Since it captures electrons from the conduction band ( $E_{CB}$ ) and holes left behind by the electrons from the valence band ( $E_{VB}$ ). This prevents the

immediate recombination of charge carriers under illumination while it reduces the number of mobile charge carriers which leads to the negative photoconductivity.

The  $I_p$  and  $I_d$  values of grown LAM crystal at 50 V are  $1.2269 \times 10^{-10}$  and  $1.9178 \times 10^{-10}$  A, respectively. The photosensitivity ( $S$ ) of grown LAM crystal can be measured from the relation:

$$S = \frac{(I_p - I_d)}{I_d} = \frac{I_{ph}}{I_d} \quad (9)$$

where  $I_{ph}$  is equal to the difference of ( $I_p - I_d$ ),  $I_p$  and  $I_d$  is photocurrent and dark current, respectively. From the relation (9), the photosensitivity ( $S$ ) of LAM crystal is obtained 0.36 at 50V. The negative photoconductivity anomaly observed for some materials like L-Proline Trichloroacetate, L-Proline Picrate, L-Proline Succinate, L-Alanine Oxalate etc. [12, 45-47]. So, it can be concluded that the material which shows the negative photoconductivity, can be used in numerous applications purposes like photo sensors and switches etc.

### 3.7. Dielectric and conductivity study

To know the electrical behavior of solids, dielectric measurement is one of the elemental characterisations. Particularly for nonconducting material, the dielectric behaviour is linked with the electro-optic properties of the crystal. For measurement, a well-polished LAM crystal is selected and then coated on both sides by using high-grade silver paste, which acts as a parallel plate capacitor. Figure 8 (a) and 8 (b) show the variation of dielectric constant and dielectric loss of LAM single crystal at a various temperature range (308 to 358 K) and range of frequency from (2 kHz to 1 MHz). From Fig. 8 (a), we observed that the value of dielectric constant is high at low frequency region and decreases rapidly with frequency range and remains constant at higher frequency range. The higher value of dielectric constant at low frequencies is due to the presence of four types of polarizations (i.e. space-charge, orientational, ionic, and electronic polarizations) [48-50]. As we increase frequency, the value of dielectric constant gets decreased, as the induced dipoles are not able to chase the variation of the applied electric field. Therefore, space-charge polarization and orientational polarization do not contribute at a higher frequency, and only ionic and electronic polarization contributes to the low value of dielectric constant. In Fig. 8 (a), it is also observed the dielectric constant increased with temperature which happens due to the hopping of the charge carriers in the lattice sites which get thermally activated [51]. From Fig. 8 (b), it can be observed that the dielectric loss value ( $\tan \delta$ ) is decreasing with increased frequency range. The large value of dielectric loss at lower frequencies is due to the polarisation of trapped charge carriers. However, at higher frequency region, the dielectric loss decreases due to the reduction of the contribution of various types of polarisation. At low frequencies, dielectric response peak in dielectric loss, is attributed to response time ( $\tau = 1 / \omega_{max}$ ) [52]. The low value of dielectric loss suggests that the LAM crystal has fewer defects/impurities, and it reveals that the grown crystal has good optical quality from the transmittance analysis which is an important property for the NLO applications [53, 54].

1  
2 Due to the presence of the  $\pi$ -electron conjugated system, these organic crystals behave like an insulator in the high  
3 purity state and its conductivity is lesser than  $ca\ 10^{-14}$  ohm.  $cm^{-1}$  at RT or below. However, defects induced by the addition  
4 of impurities in these crystals can make them behave like a semiconductor at a moderate temperature [53]. The AC  
5 conductivity ( $\sigma_{ac}$ ) is calculated by dielectric data at different temperature using the equation [55]:  
6  
7  
8

$$\sigma_{ac} = \omega \epsilon_0 \epsilon_r \tan \delta \quad (10)$$

9  
10  
11  
12  
13  
14 where  $\omega$  is the angular frequency (is equal to  $2\pi f$ ,  $f$  is frequency of the applied field),  $\epsilon_0$  is the permittivity of free  
15 space charge carriers ( $8.8541 \times 10^{-12}$  Farad/meter),  $\epsilon_r$  is the relative permittivity and  $\tan \delta$  is a dielectric loss. As shown  
16 in Fig. 9, the  $\sigma_{ac}$  is frequency dependent and increases linearly with frequency and temperature. The increase in  $\sigma_{ac}$  with  
17 frequency is correlated with the polaron hopping. As the conduction is possible by the mechanism of the hopping of  
18 charge carriers, the mobility determines the hopping rate. The drift mobility of the charge carriers and the carrier density  
19 are affected due to the defects. The defects play a significant role in the electrical conduction mechanism of such a system,  
20 as thermally ionized charged carriers get released from these defects, resulting in increase of conductivity. The topology  
21 of an organic molecule also affects its conductivity. At low temperature, there is low electrical conduction of LAM crystal,  
22 caused by the trapping of charge carriers at defect sites which is illustrated in Fig. 9. With the increase in temperature,  
23 more carriers are available due to thermal activation, and there is an increase in conductivity [56].  
24  
25  
26  
27  
28  
29  
30  
31  
32  
33  
34

### 3.8. Z-Scan study

35  
36  
37 An effective tool for measuring nonlinear refraction (NLR), nonlinear absorption coefficient (NLA), and third-  
38 order nonlinear optical susceptibility ( $\chi^{(3)}$ ) is the Z-scan method. The nonlinear refractive index ( $n_2$ ) and nonlinear  
39 absorptive properties can be revealed through closed and open aperture Z-scan experiments. Generally, nonlinear optical  
40 absorption (NLOA) is classified into two types: (i) saturable absorption (SA), which includes multiphoton absorption in  
41 which, with increases in optical intensity, transmittance of the sample increases, and (ii) reverse saturable absorption  
42 (RSA), which includes two-photon absorption (2PA) in which, with increase in optical intensity, transmittance decreases.  
43  
44  
45  
46  
47  
48

49 The sample is moved along the direction of the propagation of the laser beam from  $-Z$  to  $+Z$  position with  $Z = 0$   
50 is the focal point. At the open aperture (OA) and closed aperture (CA) conditions, the transmitted intensity was measured.  
51 The open aperture, closed aperture and ratio of closed to open (C/O) normalized Z-scan curve for LAM crystal are shown  
52 in Fig. 10. The open aperture (OA) Z-scan curve of grown LAM crystal is depicted in Fig. 10 (a), the experimental results  
53 illustrate the sample shows the RSA with positive absorption coefficient ( $\beta$ ) which affirms the occurrence of the two  
54 photon absorption (2PA) process in grown LAM crystal [57]. To obtain required parameters for optical limiting  
55 applications (OLA), this is required documentation. Materials which exhibit saturable absorption (SA) have maximum  
56  
57  
58  
59  
60

1  
2 transmittance in focus at valley while RSA exhibiting materials has minimum transmittance (T) in the focus at the valley.  
3  
4 The peak followed by a valley transmittance (T) in the closed aperture (CA) Z-scan curve as displayed in Fig. 10 (b)  
5 demonstrates the signature of negative nonlinearity cause the self-defocusing effect (SDE) [58]. The cause of self-  
6 defocusing effect (SDE) is the local variation of refractive index ( $n_2$ ) with temperature. The nonlinear optical coefficients  
7 are measured using standard equations [59] and cited in Table 3.  
8  
9  
10

#### 11 12 13 **4. Conclusions** 14

15  
16 In summary, single crystals of LAM have been successfully grown by a slow evaporation solution growth technique.  
17  
18 The confirmation of the crystal structure system is affirmed from the SCXRD analysis that the grown LAM crystal belongs  
19 to orthorhombic structure with non-centro symmetry space group  $P2_12_12_1$ . From PXRD study, good crystallinity is  
20 confirmed of the grown LAM crystal. Optical constants are calculated from the UV-Visible-NIR spectral analysis and  
21 high optical transparency is observed in the entire visible region and wide band gap (5.09 eV) of LAM crystal. From  
22 theoretical calculation, the positions of the valence band and conduction band for LAM crystal have also been  
23 investigated. The shock damage threshold of LAM single crystal is evaluated, and bubble-like projection were found to  
24 appear after applying the shock waves with a Mach number of 2.2. The thermal parameters are estimated from  
25 photoacoustic spectroscopy. The negative photoconductivity is also found for LAM single crystal. The variation in  
26 dielectric constant and dielectric loss is considered with varying frequencies and at different temperature ranges. The  
27 nonlinear parameters of LAM crystal have been evaluated from the Z-scan study, which affirmed that the nonlinearity is  
28 in the form of self-defocusing and two photon absorption (2PA) with reverse saturable absorption.  
29  
30  
31  
32  
33  
34  
35  
36  
37  
38  
39  
40

#### 41 **Conflicts of interest** 42

43 There are no conflicts of interest to declare.  
44  
45  
46

#### 47 **Acknowledgment** 48

49 Authors wish to acknowledge X-Ray Crystallographic Facility, School of Pure & Applied Physics, Mahatma Gandhi  
50 University, Kerala for Single crystal X-ray diffraction analysis. Authors are thankful to Dr. S. A. Martin Britto Dhas,  
51 Assistant Professor, Department of Physics, Sacred Heart College, Tirupattur, Vellore for shock damage threshold  
52 measurement and for good discussions. The authors are highly grateful to the Department of Physics and Centre for  
53 Nanoscience and Nanotechnology (CNN), Jamia Millia Islamia, New Delhi for facilities for the synthesis and PXRD  
54 respectively. Apurva Gupta acknowledges the University Grant Commission (UGC), Government of India for the Non-  
55 NET fellowship.  
56  
57  
58  
59  
60

## References

- [1] Rani R, Thukral K, Krishna A, Sharma G, Vijayan N, Rathi B and Bhagavannarayana G 2014 Synthesis and nucleation studies on l-leucine hydrobromide: a promising nonlinear optical material *J. Appl. Cryst.* **47** 1966-1974
- [2] Krishna A, Vijayan N, Verma S, Singh B, Bidkin I, Jayalakshmy M S, Sridhar B and Das S 2017 Crystalline perfection, thermal, mechanical and optical investigations on solution grown l-arginine monohydrochloride single crystal *J Mater Sci: Mater. Electron* **28** 4306-43112
- [3] Yadav H, Sinha N and Kumar B 2014 Growth and characterization of piezoelectric benzil single crystals and its application in microstrip patch antenna. *Cryst Eng Comm.* **16** 10700-10710
- [4] Souza T E, Rosa I M L, Legendre A O, Paschoal D, Maia L J, Santos H F D, Martins F T and Doriguetto AC 2015 Non-centrosymmetric crystals of new N-benzylideneaniline derivatives as potential materials for non-linear optics *Acta Cryst gra. B* **71** 416-426
- [5] Sangeetha K, Babu R R, Kumar P, Bhagavannarayana G and Ramamurthi K, 2011 Effect of H<sup>+</sup> ion implantation on structural, morphological, optical and dielectric properties of l-arginine monohydrochloride monohydrate single crystals *Appl. Surf. Sci.* **257** 7573-7578
- [6] Chemla D S and Zyss J Nonlinear Optical Properties of Organic Molecules and Crystals Academic Press. New York, 1987)
- [7] Thukral K, Vijayan N, Haranath D, Maurya KK, Philip J and Jayaramakrishnan V 2015 Comprehensive study on l-Proline Lithium Chloride Monohydrate single crystal: A semiorganic material for nonlinear optical applications. *Arabian J. Chem.* <http://dx.doi.org/10.1016/j.arabjc.2015.08.022>
- [8] Thukral K, Vijayan N, Haranath D, Jayaramakrishnan V, Philip J, Sreekanth P and Bhagavannaryana, G 2015 Assessment on third order nonlinearity and other optical analyses of L-Asparagine Monohydrate single crystal: An efficient candidate for harmonic conversions *Spectrochimica Acta Part A: Mol. Biomol. Spectrosc.* **151** 419-425.
- [9] Kathiravan P and Balakrishnan T, 2015 Growth and characterization of pure and cesium-doped L-asparagine monohydrate single crystals *Struct Chem Crystallogr Commun* **1**,19 ISSN 2470-9905
- [10] Shakir M, Kushawaha S K, Maurya K K, Kumar S, Wahab M A and Bhagavannarayana G 2010 Enhancement of second harmonic generation, optical and dielectric properties in L-asparagine monohydrate single crystals due to an improvement in crystalline perfection by annealing *J. Appl. Cryst.* **43** 491-497
- [11] Kalaiselvi D, Kumar R M and Jayavel R 2008 Crystal growth, thermal and optical studies of semiorganic nonlinear optical material: L-lysine hydrochloride dihydrate *Mater. Res. Bull.* **43** 1829-1835

- 1  
2 [12] Thukral K, Vijayan N, Krishna A, Singh B, Kant R, Jayaramkrishnan V, Jayalakshmy M S and Kaur M 2016 In-  
3 depth behavioral study of l-Proline Trichloroacetate single crystal: An efficient candidate for NLO applications.  
4 *Arab. J. Chemi.* <http://dx.doi.org/10.1016/j.arabjc.2016.09.011>  
5  
6  
7 [13] Natarajan S, Umamaheswaran M, Sundar JK, Suresh J and Dhas S M B 2010 Structural, spectroscopic and nonlinear  
8 optical studies on a new efficient organic donor–acceptor crystal for second harmonic generation: l-Threoninium  
9 picrate *Spectrochim. Acta Part A* **77** 160–163  
10  
11  
12 [14] Kripal R and Singh P 2007 EPR and optical absorption studies of VO<sup>2+</sup> ions in L-asparagine monohydrate *Solid state*  
13 *commun.* **142** 412-416  
14  
15  
16 [15] Yadav H, Sinha N and Kumar B, 2015 Growth and characterization of new semiorganic nonlinear optical and  
17 piezoelectric lithium sulfate monohydrate oxalate single crystals. *Mater. Res. Bull.* **64** 194-199  
18  
19  
20 [16] Srineevasan R, Anbarasi A, Revathi T and Kumar S R 2016 Growth and characterizations of a new semiorganic  
21 nonlinear optical material thiourea potassium hydrogen phthalate for NLO applications. *Mater. Chem. Phys.* **177** 25-  
22 30  
23  
24  
25 [17] Moovendaran K and Natarajan S 2013 Unidirectional growth and characterization of L-tartaric acid single crystals *J.*  
26 *Appl. Cryst.* **46** 993-998  
27  
28  
29 [18] Jaikumar D, Kalainathan S and Bhagavannarayana G 2010 Structural, spectral, thermal, dielectric, mechanical and  
30 optical properties of urea l-alanine acetate single crystals. *Physica B: Condensed Matter.* **405** 2394-2400  
31  
32  
33 [19] Jauhar R M, Viswanathan V, Vivek P, Vinitha G, Velmurugan D and Murugakoothan P 2016 A new organic NLO  
34 material isonicotinamidium picrate (ISPA): crystal structure, structural modeling and its physico-chemical properties.  
35 *RSC Advan.* **6** 57977-57985  
36  
37  
38 [20] Thukral K, Vijayan N, Rathi B, Bhagavannarayana G, Verma S, Philip J, Krishna A, Jeyalakshmy M S and Halder S  
39 K 2014 Synthesis and single crystal growth of L-proline cadmium chloride monohydrate and its characterization for  
40 higher order harmonic generation applications. *Cryst. Eng. Comm.* **16** 2802-2809  
41  
42  
43 [21] Dalal J and Kumar B 2016 Bulk crystal growth, optical, mechanical and ferroelectric properties of new semiorganic  
44 nonlinear optical and piezoelectric Lithium nitrate monohydrate oxalate single crystal *Optical Mater.* **151** 139-147  
45  
46  
47 [22] Vierzbicke B D, Patel S, Davis B E and Birnie III D P 2015 Evaluation of the Tauc method for optical absorption edge  
48 determination: ZnO thin films as a model system. *Phys. Status Solidi B* **252** **8** 1700-1710  
49  
50  
51 [23] Parrey K A, Aziz A, Ansari S G, Mir S H, Khosla A and Niazi A 2018 Synthesis and Characterization of an Efficient  
52 Hole-Conductor Free Halide Perovskite CH<sub>3</sub>NH<sub>3</sub>PbI<sub>3</sub> Semiconductor Absorber Based Photovoltaic Device for IOT  
53 *J. Electrochem. Socie. B* **165** 3023-3029  
54  
55  
56 [24] Shkir M, Muhammad S, AlFaify S, Irfan A and Yahia I S 2015 A dual approach to study the electro-optical properties  
57 of a noncentrosymmetric l-asparagine monohydrate. *Spectrochim. Acta Part A: Mol. Biomol. Spectrosc.* **137** 432-441  
58  
59  
60

- 1  
2 [25] Vasudevan P, Raj S G and Sankar S 2013 Synthesis and characterization of nonlinear optical L-arginine semi-  
3 oxalate single crystal. *Spectrochim Acta Part A: Mol. Biomol. Spectrosc.* **106** 210-215  
4  
5 [26] Jayanthi L, Prabavathi N, Sivasubramani V, Pandian M S, Ramasamy P and Dhas S M B 2017 Bulk growth of  
6 organic 4-hydroxy l-proline (HLP) single crystals grown by conventional slow evaporation and Sankaranarayanan-  
7 Ramasamy (SR) method *J Mater Sci: Mater. Electron* **28** 15354-15369  
8  
9 [27] Hassanien A S and Akl A A 2016 Effect of Se addition on optical and electrical properties of chalcogenide CdSSe  
10 thin films *Super. Microstru.* **89** 153-169  
11  
12 [28] Xing C, Zhang Y, Yan W, Guo L, Xing C, Zhang Y, Yan W and Guo L 2006 Band structure-controlled solid solution  
13 of Cd<sub>1-x</sub>Zn<sub>x</sub>S photocatalyst for hydrogen production by water spilling *Intern. J. Hydro. Ener.* **31** 2018 – 2024  
14  
15 [29] Askari M, Soltani N, Saion E, Yunus W M M, Erfani H M and Dorostkar M 2015 Structural and optical properties  
16 of PVP-capped nanocrystalline Zn<sub>x</sub>Cd<sub>1-x</sub>S solid solutions *Super. Microstru.* **81** 193-201  
17  
18 [30] Karuppasamy P, Pandian M S, Ramasamy P and Verma S 2018 Crystal growth, structural, optical, thermal,  
19 mechanical, laser damage threshold and electrical properties of triphenylphosphine oxide 4-nitrophenol (TP4N)  
20 single crystals for nonlinear optical applications. *Optical Materials* **79** 152-171  
21  
22 [31] Herzberg G and Monfils A 1961 The Dissociation Energies of the HP, HD, and DZ Molecules *J. Mol. Spectroscopy*  
23 **5** 1-6  
24  
25 [32] Sonia, Vijayan N, Vij M, Krishna A, Yadav H, Maurya, K.K, Dhas S M B and Kumar P 2019 An efficient piezoelectric  
26 single-crystal l-argininium phosphite: structural, Hirshfeld, electrical and mechanical analyses for NLO  
27 applications *Applied Physics A*, **125** 363  
28  
29 [33] Sonia, Vijayan N, Vij M, Yadav H, Kumar R, Sur D, Singh B, Dhas S M B and Verma S 2019 Evaluation of structural,  
30 optical and mechanical behaviour of L-argininium bis (trifluoroacetate) single crystal: An efficient organic material  
31 for second harmonic generation applications. *J. Phys. and Chem. of Solids*, **129**, 401-412  
32  
33 [34] Jagadeesh G 2008 Fascinating world of shock waves *Resonance* **13** 752-767  
34  
35 [35] Sonia, Vijayan N, Bhushan M, Thukral K, Raj R, Maurya K K, Haranath D and Dhas S M B 2017 Growth of a  
36 bulk-size single crystal of sulphamic acid by an in-house developed seed rotation solution growth technique and its  
37 characterization *J. Appl. Cryst.* **50** 763–768  
38  
39 [36] Dhas S M B, Suresh M, Raji P, Ramachandran K and Natarajan S 2007 Photoacoustic studies on two new organic  
40 NLO materials: L-threonine and L-prolinium tartrate *Cryst. Res. Technol* **42** 190-194  
41  
42 [37] Saranraj A, Dhas S S, Jose M, Dhas S M B 2018 Growth of bulk single crystals of urea for photonic applications.  
43 *Electron. Mater. Lett.* **14** 7-13  
44  
45 [38] Melo W B and Faria R M 1995 Photoacoustic procedure for measuring thermal parameters of transparent solids  
46 *Appl. Phys. Lett.* **67** 3892-3894  
47  
48  
49  
50  
51  
52  
53  
54  
55  
56  
57  
58  
59  
60

- 1  
2 [39] Manivannan M, Dhas S M B and Jose M 2016 Photoacoustic and dielectric spectroscopic studies of 4-  
3 dimethylamino-n-methyl-4-stilbazolium tosylate single crystal: an efficient terahertz emitter. *J. Cryst. Growth* **455**  
4 161-167  
5  
6  
7 [40] Kim Y 2000 Physical, chemical and optical properties of aqueous L-arginine phosphate (LAP) solution *J. Mater. Sci.*  
8 **35** 873-880  
9  
10  
11 [41] Loiacono G M, Kostecky G 1981 Thermal properties of Pure and Doped TGS, DTGS, TGFB and DTGFB single  
12 crystals. *Mat. Res. Bull.* **16** 53-58  
13  
14 [42] Ambujam K, Selvakumar S, Prem Anand D, Mohamed G and Sagayaraj P 2006 Crystal growth, optical, mechanical  
15 and electrical properties of organic NLO material  $\gamma$ -glycine. *Cryst. Res. Technol.* **41** 671 – 677  
16  
17 [43] Bube R H, Photoconductivity of Solids, New York (1981)  
18  
19 [44] V.N. Joshi, Photoconductivity, Marcel Dekker, New York (1990)  
20  
21 [45] Thukral K, Vijayan N, Vij M, Nagaraja C M, Jayaramakrishnan V, Jayalakshmy M S and Kant R 2017 Analyses of  
22 significant features of L-Proline Picrate single crystal: An excellent material for nonlinear optical applications  
23 *Mater. Chem. Phys.* **194** 90-96  
24  
25 [46] Balamurugaraj P, Suresh S, Koteeswari P and Mani P 2013 Growth, Optical, Mechanical, Dielectric and  
26 Photoconductivity Properties of L-Proline Succinate NLO Single Crystal *J. Mater. Phys. Chem.* **1** 4-8  
27  
28 [47] Arun K J and Jayalakshmi S 2009 Growth and Characterisation of Nonlinear Optical Single Crystals of L-Alanine  
29 Oxalate *J. Miner. Mater. Charact. Eng.* **8** 635-646  
30  
31 [48] Kalidasan M, Asokan K, Baskar K and R. Dhanasekaran 2015 Effect of gamma ray irradiation on sodium borate  
32 single crystals *Radia. Phys. Chemi.* **117** 70–77  
33  
34 [49] Rani N, Vijayan N, Riscob B, Jat S K, Krishna A, Das S, Bhagavannarayana G, Rathi B and Wahab M A 2013 Single  
35 crystal growth of ninhydrin by unidirectional Sankaranarayanan–Ramasamy (SR) method by using a glass ampoule  
36 for nonlinear optical applications *Cryst Eng Comm* **15** 2127–2132  
37  
38 [50] Riscob B, Kushwaha SK, Shakir M, Nagarajan K, Maurya K K, Haranath D, Roy S D and Bhagavannarayana G 2011  
39 Crystalline perfection, optical and dielectric studies on L-histidine nitrate: A nonlinear optical material *Physica B* **406**  
40 4440–4446  
41  
42 [51] Krishnakumar V, Avasthi DK, Singh F, Kulriya P K and Nagalakshmi R 2007 Study of the damage produced in K [CS  
43  $(\text{NH}_2)_2$ ]  $4\text{Br}$ —a non-linear optical single crystal by swift heavy ion irradiation, *Nucl. Instru. Methods Phys Res. B*  
44 **256** 675–682  
45  
46 [52] Adhlakha N, Yadav K L and Singh R 2014 Effect of  $\text{BaTiO}_3$  addition on structural, multiferroic and magneto-  
47 dielectric properties of  $0.3 \text{CoFe}_2\text{O}_4$ – $0.7 \text{BiFeO}_3$  ceramics. *Smart Mater. Struct.* **23** 105024  
48  
49  
50  
51  
52  
53  
54  
55  
56  
57  
58  
59  
60

1  
2  
3  
4  
5  
6  
7  
8  
9  
10  
11  
12  
13  
14  
15  
16  
17  
18  
19  
20  
21  
22  
23  
24  
25  
26  
27  
28  
29  
30  
31  
32  
33  
34  
35  
36  
37  
38  
39  
40  
41  
42  
43  
44  
45  
46  
47  
48  
49  
50  
51  
52  
53  
54  
55  
56  
57  
58  
59  
60

- [53] Yadav H, Sinha N, Goel S, Singh B, Bdikin I, Saini A, Gopalaiah K and B. Kumar 2017 Growth, crystal structure, Hirshfeld surface, optical, piezoelectric, dielectric and mechanical properties of bis (L-asparaginium hydrogensquarate) single crystal *Acta Crystgra. B* **73** 347–359
- [54] Yadav H, Sinha N, Tyagi N and Kumar B 2015 Enhancement of optical, piezoelectric, and mechanical properties in crystal violet dye-doped benzophenone crystals grown by Czochralski technique *Cryst. Growth Des.* **15** 4908–4917
- [55] Habib Z, Ikram M, Majid K and Asokan K 2014 Structural, dielectric and ac conductivity properties of Ni-doped  $\text{HoFeO}_3$  before and after gamma irradiation. *Appl. Phys. A* **116** 1327–1335
- [56] Tyagi N, Sinha N and Kumar B 2014 Evidence of sustained ferroelectricity in glycine sodium nitrate single crystal. *Current Appl. Phys.* **14** 156-160
- [57] Jauhar RM, Kalainathan S and Murugakoothan P Three dimensional organic framework of 2-amino 4, 6 dimethoxypyrimidine p-toluenesulfonic acid monohydrate: synthesis, single crystal growth and its properties *J. Cryst. Growth* **424** 42-48
- [58] Suresh A, Manikandan N, Jauhar R M, Murugakoothan P and Vinitha G 2018 Growth and characterizaion of urea p-nitrophenol crystal: an organic nonlinear optical material for optoelectronic device application *Appl. Phys. A* **124** 419 <https://doi.org/10.1007/s00339-018-1767-2>
- [59] Dhanaraj P V, Rajesh N P, Sundar J K, Natarajan S and Vinitha G 2011 Studies on growth, crystal structure and characterization of novel organic nicotinium trifluoroacetate single crystals *Mater. Chemi. Phys.* **129** 457–463

Accepted Manuscript

## Figures and Tables

### Figures captions:

Figure 1. Image of polished LAM single crystal.

Figure 2. PXRD pattern of LAM single crystal.

Figure 3. (a) UV-Visible-NIR transmittance spectrum of LAM crystal (inset absorption spectrum of LAM single crystal), and (b) Tauc plot of  $(\alpha h\nu)^2$  vs. photon energy ( $h\nu$ ) for band gap calculation.

Figure 4. Valence band and conduction band positions of LAM single crystal.

Figure 5. Optical microscopic image of before and after shock of grown LAM single crystal.

Figure 6. The variation of PA signal with different chopping frequency of LAM crystal.

Figure 7. The variation of photocurrent ( $I_p$ ) and dark current ( $I_d$ ) with applied electric field.

Figure 8. The variation of a dielectric constant and dielectric loss of LAM crystal (a & b) over the frequency range 2 kHz-1 MHz at different temperature 308-358 K.

Figure 9. The variation of AC conductivity ( $\sigma_{ac}$ ) versus frequency of LAM crystal at a different temperature range (308 K-358 K).

Figure 10. The normalized transmittance (T) with open aperture (OA) and closed aperture (CA) conditions as a function of distance Z-along the lens axis in the far field of LAM crystal (a) and (b), and (c) the ratio of closed to open (C/O) curve.

### Tables

Table 1. Comparison of the lattice parameter with values from the literature:

Table 2. Calculated thermal parameters of LAM crystal by the photoacoustic measurement.

Table 3. Optimized parameters while performing Z-Scan measurement.

Table 1

Sample name	a (Å)	b (Å)	c (Å)
LAM single crystal (Reported value ref. 14)	5.593	9.827	11.808
LAM single crystal (observed vale)	5.596	9.840	11.808
Difference	0.003	0.013	0

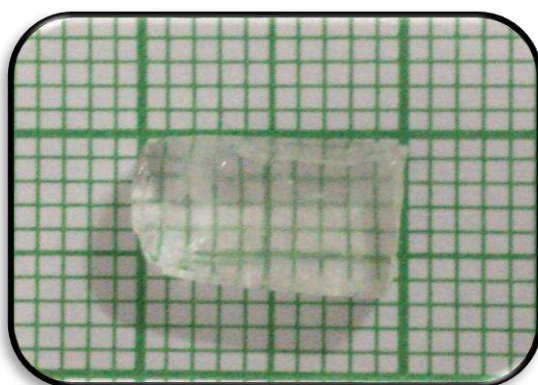
Table 2

Sample name	Diffusivity ( $\times 10^{-6} \text{ m}^2 \text{ s}^{-1}$ )	Conductivity ( $\text{W m}^{-1} \text{ K}^{-1}$ )	Effusivity ( $\text{m}^2 \text{ K}^{-1} \text{ s}^{-1/2}$ )
LAM crystal	4.099	1.370	676.665

Table 3

Parameters	Measured value
Wavelength of laser beam ( $\lambda$ )	532 nm
Laser power input (P)	100 mW
Thickness of sample	1 mm
Nonlinear refractive index ( $n_2$ )	$5.06 \times 10^{-10} \text{ cm}^2/\text{W}$
Nonlinear absorption coefficient ( $\beta$ )	$1.04 \times 10^{-5} \text{ cm}/\text{W}$

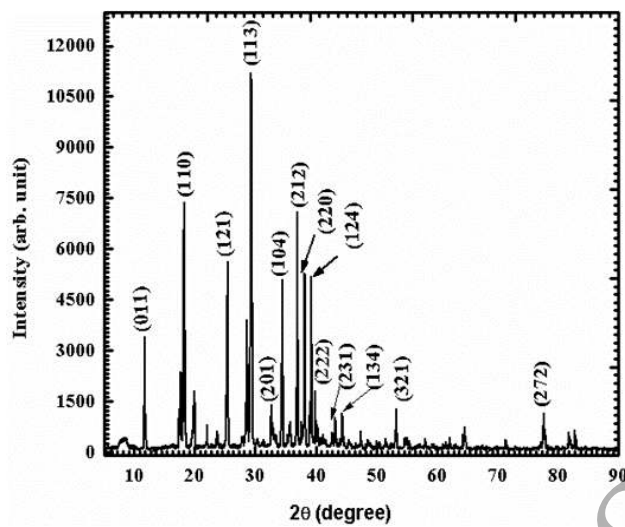
Figure 1



Accepted Manuscript

1  
2  
3  
4  
5  
6  
7  
8  
9  
10  
11  
12  
13  
14  
15  
16  
17  
18  
19  
20  
21  
22  
23  
24  
25  
26  
27  
28  
29  
30  
31  
32  
33  
34  
35  
36  
37  
38  
39  
40  
41  
42  
43  
44  
45  
46  
47  
48  
49  
50  
51  
52  
53  
54  
55  
56  
57  
58  
59  
60

Figure 2



Accepted Manuscript

Figure 3

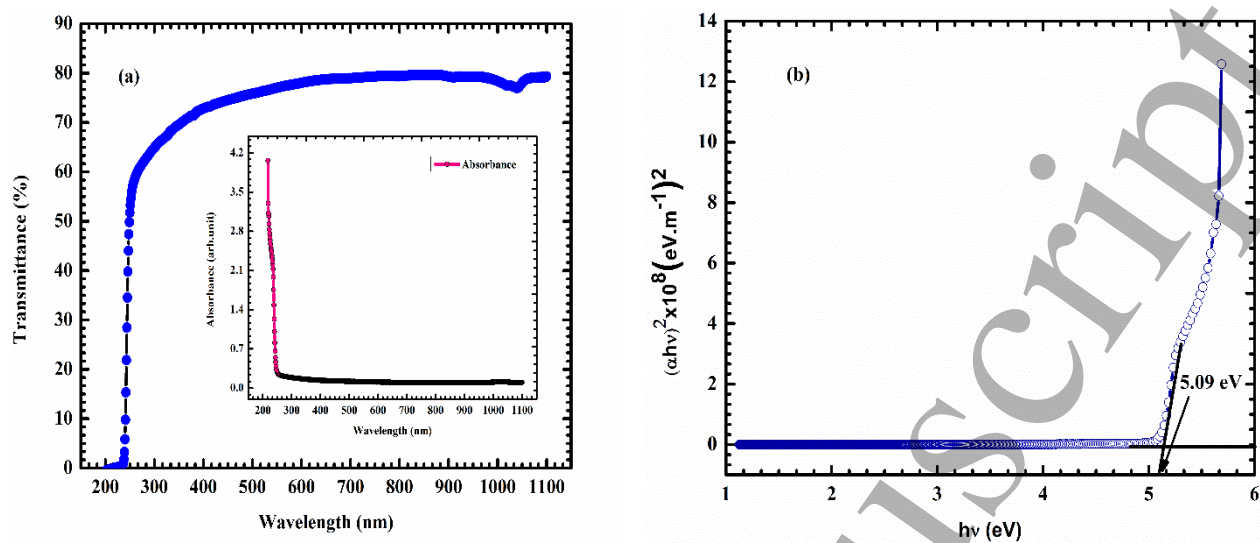
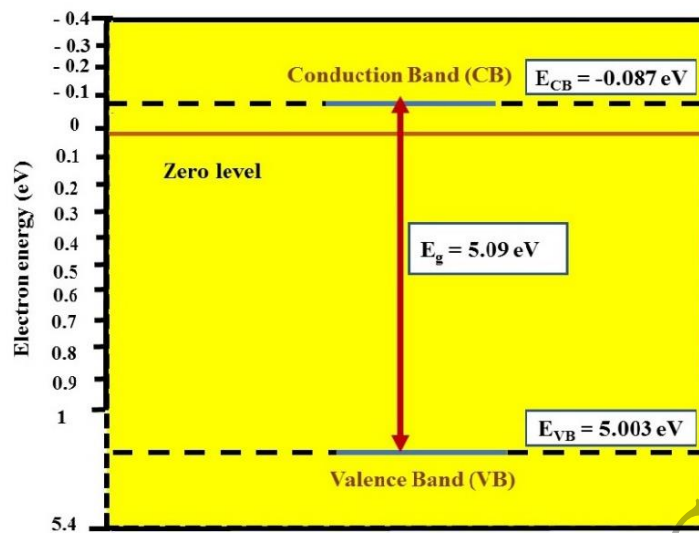


Figure 4



Accepted Manuscript

Figure 5

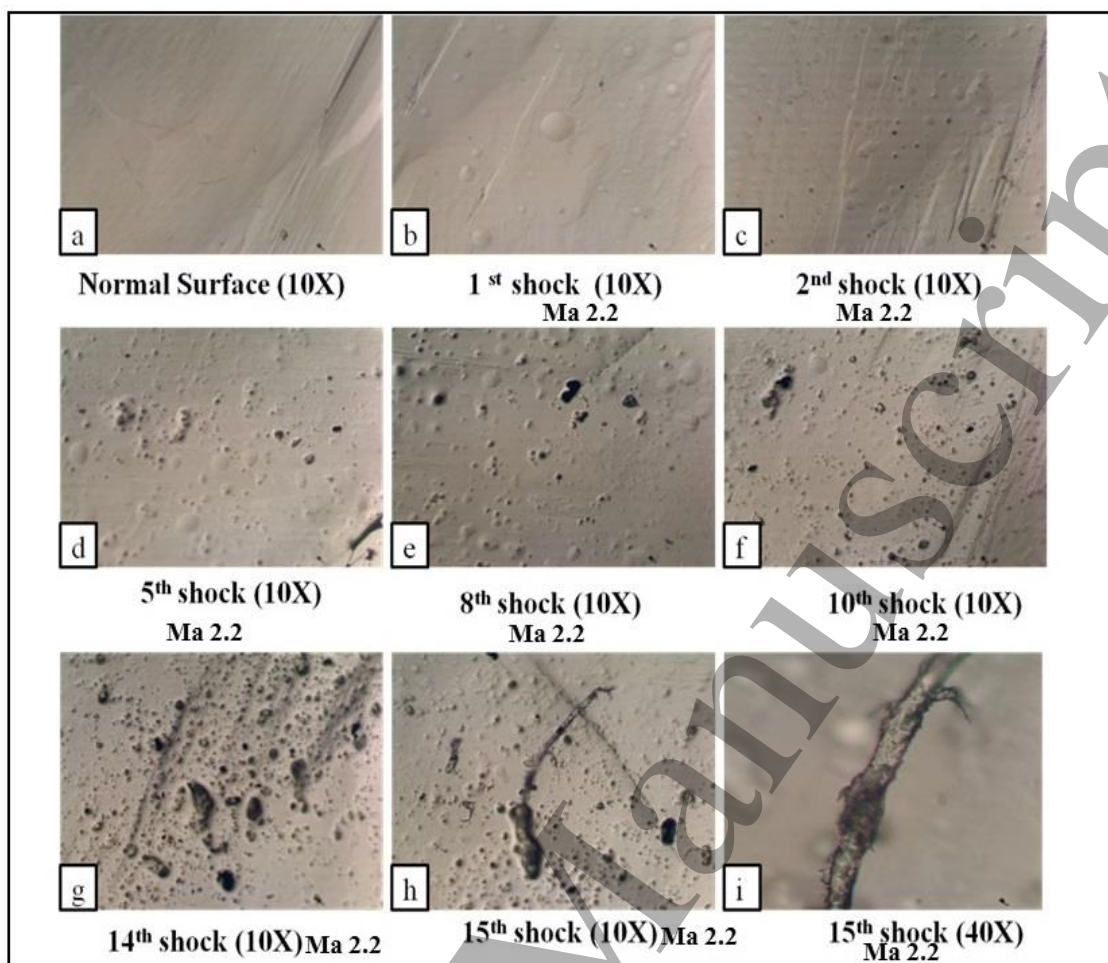
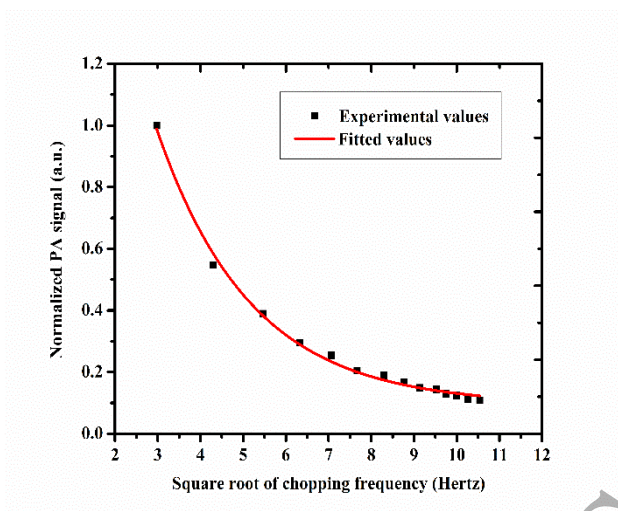


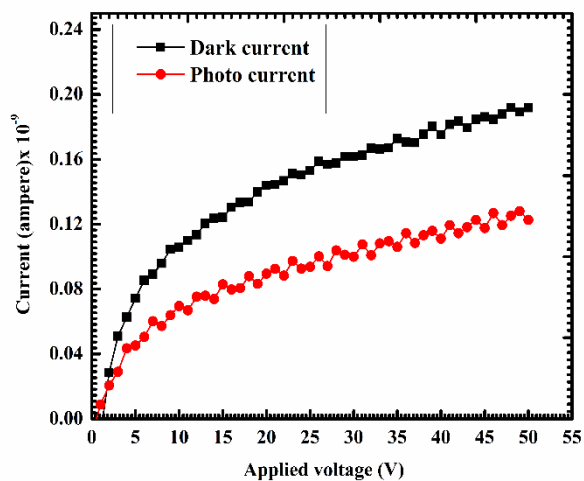
Figure 6



Accepted Manuscript

1  
2  
3  
4  
5  
6  
7  
8  
9  
10  
11  
12  
13  
14  
15  
16  
17  
18  
19  
20  
21  
22  
23  
24  
25  
26  
27  
28  
29  
30  
31  
32  
33  
34  
35  
36  
37  
38  
39  
40  
41  
42  
43  
44  
45  
46  
47  
48  
49  
50  
51  
52  
53  
54  
55  
56  
57  
58  
59  
60

Figure 7



Accepted Manuscript

Figure 8

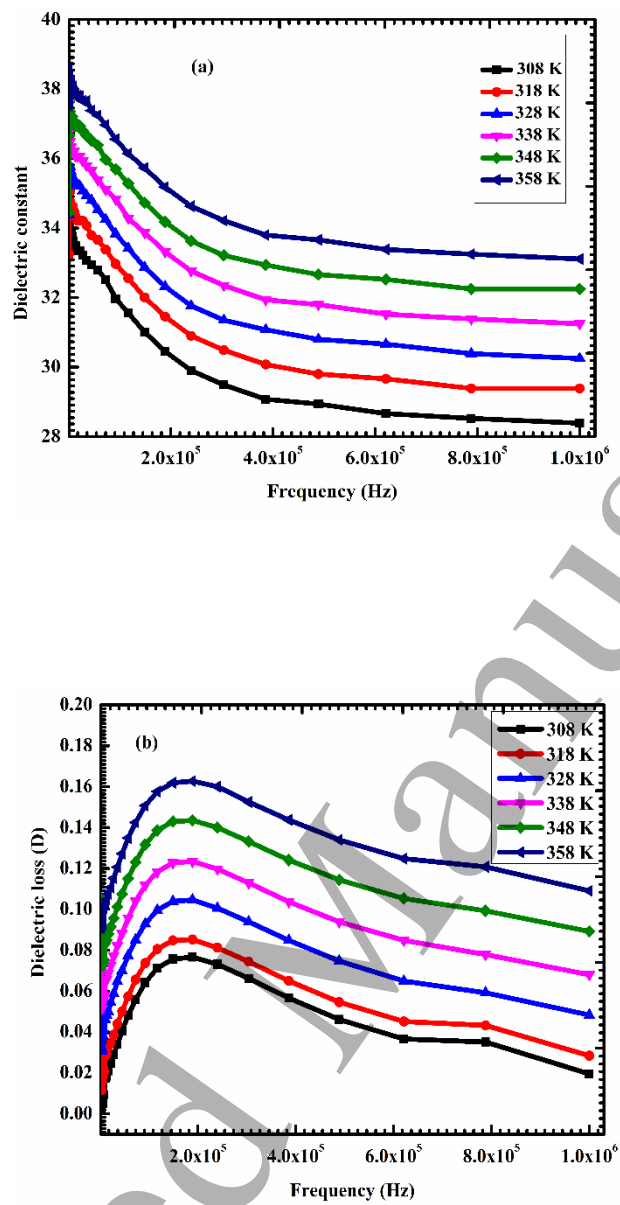


Figure 9

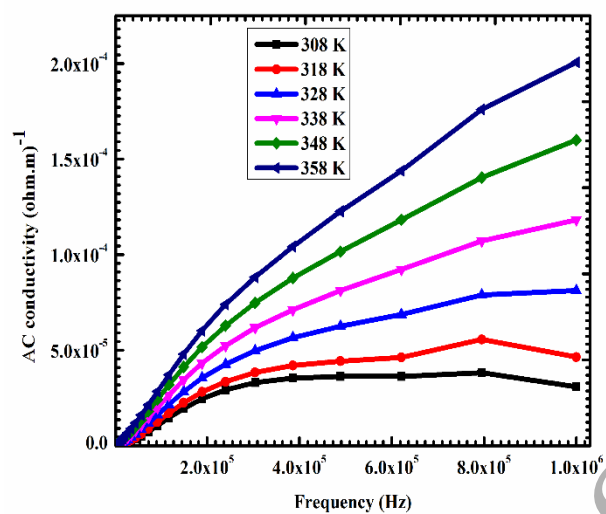


Figure 10

